The medium amplitude oscillatory shear of semi-dilute colloidal dispersions, part 2: third harmonic stress contribution

James W. Swan[1]*, A. Kate Gurnon[2] and Norman J. Wagner[2]
[1]Department of Chemical Engineering
Massachusetts Institute of Technology, Cambridge, MA
[2]Department of Chemical and Biomolecular Engineering
University of Delaware, Newark, DE

April 9, 2015

Synopsis

In a companion paper [Swan, Furst and Wagner (JOR, 2014)] we derived an exact theoretical description of medium amplitude oscillatory shear (MAOS) for a semi-dilute colloidal dispersion. Through solution of the Smoluchowski equation governing the spatial distribution of suspended particles in the semi-dilute limit, we calculated the stresses that arise from an oscillatory linear flow as an expansion in powers of the rate of deformation. Here, this is extended to calculation of the first departures from linearity in the first and third harmonics of the suspension stress driven by oscillatory deformation. The role of hydrodynamic interactions is investigated via the excluded-annulus model in which particles are given an impenetrable core with a radius larger than their hydrodynamic radius. The ratio of these length scales controls the strength of hydrodynamic interactions. The third harmonic of the suspension stress is predicted to be dominated by hydrodynamic stresses at high frequency, a result that is shown to be valid experimentally for the oscillatory shear response of concentrated near hard-sphere dispersions. The calculations anticipate recent experimental observations on model near hard-sphere colloidal dispersions and quantitative agreement is demonstrated when the predictions are scales appropriately to account for volume fraction effects. The first departures from linearity in harmonics of the suspension stress are separated into several material functions that are independent of the flow geometry. These functions are generated from detailed numerical solutions, while asymptotic analysis is shown to predict the values of these functions at high frequency. These exact calculations provide a basis for understanding the onset of nonlinear rheological behavior of colloidal suspensions under dynamic oscillatory flow.

I Introduction

Large amplitude oscillatory shear (LAOS) is an experimental methodology for probing the nonlinear and time dependent rheology of non-Newtonian fluids [Dealy and Wissbrun (1990)]. With this method, a complex fluid is deformed in an oscillatory fashion having a simple shear geometry. The rate of strain in the material is commonly written as $\dot{\gamma}_0 \cos(\omega t)$, where $\dot{\gamma}_0$ is the maximum strain rate and ω is the frequency of oscillation. The shear stress is measured in time and then represented as harmonics of the imposed deformation:

$$\sigma(t) = \sum_{n=-\infty}^{\infty} e^{in\omega t} A_n(\dot{\gamma}_0, \omega). \tag{1}$$

*Corresponding author; Electronic mail: jswan@mit.edu

Time reversal symmetry requires that $A_n(\omega) = 0$ for even values of n [Atalik and Keunings (2004)]. The remaining odd coefficients, sometimes termed harmonics, tend to decay with increasing n.

Small amplitude oscillations produce a shear stress linear in $\dot{\gamma}_0$ – the linear response of the non-Newtonian fluid under study [Pipkin (1986)]. With increasing deformation amplitude, a nonlinear response emerges that activates higher, odd harmonics of the shear stress [Giacomin and Dealy (1993)]. The behavior of these higher harmonics is not well understood except in particular limits. For instance, when $\omega \to 0$, a LAOS experiment probes the steady shear rheology of a material [Swan, Zia and Brady (2014)]. The present article focuses on another limiting case of LAOS termed medium amplitude oscillatory shear (MAOS) in which the maximum rate of deformation is small [Bird, Armstrong and Hassager (1987)]. MAOS measures the leading departures from linearity in $\dot{\gamma}_0$. These departures in the shear stress scale as $\dot{\gamma}_0^3$. This provides a basic description of the onset of non-linearity in the memory of a complex fluid [Pipkin (1986)].

The utility of LAOS for identifying particular classes of non-Newtonian fluids and generating data for fitting to constitutive models is well established [Hyun *et al.* (2002); Ewoldt, Hosoi and McKinley (2008)]. Many methods for interpreting and comparing the results of LAOS experiments have been crafted as well [Wilhelm (2002); Rogers, Kohlbrecher and Lettinga (2012)]. Recent theoretical efforts have focused on understanding the interplay of microscopic forces within a complex fluid and how those give rise to the nonlinear and time dependent stress signals that emerge from LAOS [Swan, Zia and Brady (2014); Swan, Furst and Wagner (2014); Bird et al. (2014)]. This detailed view of materials and their time dependent response is at the forefront of modern rheological investigation and experimental measurements of complex fluid microstructure under LAOS flow is now possible [Gurnon et al. (2014); Kim et al. (2014)]. The goal is to bridge length and time scales by describing the macroscopic stress in these materials in terms of the microscopic forces, structures and relaxation spectra of complex materials under time dependent deformation.

A particularly useful model of such materials is the colloidal dispersion. The stress in a suspension of hydrodynamically interacting particles has three principle contributions coming from three separate forces on the suspended particles: hydrodynamic, Brownian and inter-particle [Batchelor (1977); Brady (1993); Brady and Wagner (2009); Mewis and Wagner (2012)]. For smooth hard-spheres, the inter-particle forces are assumed to be zero since hydrodynamic lubrication prevents inter-particle contact. In other cases such as charged particles, particles coated with interacting polymer brushes, or particles suspended with non-absorbing polymer, inter-particle forces will be significant [Russel et al. (1989)]. A key question is how significant are these contributions under different flow conditions. As we will demonstrate here, MAOS provides an interesting means of addressing this question.

A theoretical approach is proposed to predict the nonlinear memory effects associated with MAOS. In particular, we study the microstructure of semi-dilute suspensions – those having only pair interactions – as a function of strain-rate amplitude, oscillation frequency and the relative strength of hydrodynamic forces. Through variation of these parameters we have found that suspensions can express a wide spectrum of nonlinear viscoelastic responses depending on flow conditions and the forces between suspended particles.

In our previous paper [Swan, Furst and Wagner (2014)], a theoretical description of the relationship between harmonics of the suspension stress and harmonics of the suspension microstructure was developed. In particular, the third harmonic of hydrodynamic contributions to the stress derives from the second harmonic of the suspension microstructure. However, the third harmonic of Brownian contributions to the stress derives from the third harmonic of the microstructure. In the high frequency limit, our asymptotic analysis suggested that the second and third harmonics of the microstructure decay in intensity as ω^{-2} and ω^{-3} respectively. We concluded that the third harmonic of the stress should be dominated by hydrodynamic contributions.

We have now performed experiments with suspensions of sub-micron silica spheres in MAOS at high frequency [Gurnon (2014)]. We find that the third harmonic of the suspension stress scales with the maximum rate of strain cubed ($\dot{\gamma}_0^3$) and inversely with the frequency squared (ω^{-2}). This scaling matches our earlier predictions. Comparisons of this behavior with some common rheological models shows a disparity. The Giesekus model, for example, predicts that the third harmonic of the shear stress scales inversely with the fourth power of frequency ω^{-4} in MAOS at high frequency [Gurnon and Wagner (2012)]. Other constitutive equations predict stronger scaling than observed in experiment as well [Giacomin and Bird (2011); Hyun *et al.* (2011)]. Our theory shows that the source of this discrepancy is the hydrodynamic interactions between colloidal particles which produce a stress that depends on the local particle configuration. This is in contrast to most models for viscoelastic fluids where the hydrodynamic stress is modeled as the product of a constant high frequency viscosity and the local rate of strain in the material. In colloidal dispersions, the hydrodynamic stress depends on the suspension structure [Batchelor and Green (1972),Brady and Bossis (1988)]. This relationship is responsible for phenomena such as shear thickening [Morris and Brady (1997)] and the observed MAOS response.

In the present paper, we construct detailed numerical solutions for the microstructure and stresses produced by MAOS and determine the third harmonic of the suspension stress as well as first departures from linearity in the first harmonic of the suspension stress. We present MAOS experiments with suspensions and show that our simple, semi-dilute model predicts the experimental behavior quantitatively. The paper is organized as follows: section II is a brief review of the proposed model, section III presents the model results as well as the comparison to experimental measurements, section IV contains concluding remarks on MAOS, LAOS and the time dependent rheology of suspensions.

II A brief review of the semi-dilute suspension model

Our previous work provides a derivation of the equations for the time dependent suspension microstructure and stress under MAOS [Swan, Furst and Wagner (2014)]. The microstructure, represented as harmonics of the pair distribution function for particles in the suspension, is reviewed in section A. The inter-particle forces directing particle motion in the suspension are reviewed in section B. The stress, represented as harmonics of the hydrodynamic, Brownian and inter-particle contributions to the suspension stress, is reviewed in section C. The first and second harmonics of the microstructure and stress were calculated in our previous work. The same calculations are extended to the third harmonics of the microstructure and stress and the first departures from linearity in the first harmonic of these same quantities in the appendix.

A Suspension microstructure

The pair-distribution function, $g(\mathbf{r},t)$, is the probability density for finding a pair of particles separated by $\mathbf{r}$ at time t divided by the particle number density. The Smoluchowski equation governs the pair distribution function in a semi-dilute suspension of hard-spheres deformed by the oscillatory flow field $\mathbf{U}(\mathbf{r})\cos(\omega t)$ with relative particle diffusivity $\mathbf{D}(\mathbf{r})$ [Batchelor (1977); Brady and Vicic (1995)]:

$$\dot{g} + \cos(\omega t)\nabla\cdot(\mathbf{U}g) = \nabla\cdot\mathbf{D}\cdot\nabla g, \tag{2}$$

with boundary conditions $g(\mathbf{r},t)\to 1$ as $\mathbf{r}\to\infty$ and

$$\hat{\mathbf{r}}\cdot\left(\mathbf{U}\cos(\omega t)g - \mathbf{D}\cdot\nabla_r g\right), \tag{3}$$

at inter-particle contact, $r=2b$ with $\hat{\mathbf{r}}=\mathbf{r}/r$. A linear flow is assumed here, $\mathbf{U}(\mathbf{r})=\dot{\mathbf{\Gamma}}\cdot\mathbf{r}-\mathbf{H}(\mathbf{r}):\mathbf{E}$ where $\dot{\mathbf{\Gamma}}$ is the shear rate amplitude tensor, $\mathbf{E}$ is the symmetric part of $\dot{\mathbf{\Gamma}}$, $\mathbf{\Omega}$ is the anti-symmetric part of $\dot{\mathbf{\Gamma}}$ and $\mathbf{H}(\mathbf{r})$ reflects the hydrodynamic coupling of particles via the shear flow. This equation describes a balance of advective and diffusive fluxes of particles which lead to

distortion of the pair-distribution function from its equilibrium state. Equations 2 and 3 are valid in the limit that the particle number density, n, goes to zero and accurate to $O(n^2)$. The stresses in a suspension are linear in integrals over the pair distribution function and will be evaluated up to $O(n^2)$ as well. This is the definition of semi-dilute. Thus knowledge of $g(\mathbf{r},t)$ as solutions to these equations is essential to determining the stress.

The following scales are adopted to make the equation dimensionless: $\mathbf{r} \sim b$, a particle's hard-sphere radius; $\mathbf{U} \sim \dot{\Gamma} b$, the characteristic flow velocity; $\mathbf{D}(\mathbf{r}) \sim D$, the characteristic relative diffusivity; and $t \sim b^2/D$. This gives rise to two dimensionless groups:

$$\mathrm{Pe} = \frac{\dot{\Gamma} b^2}{D}, \tag{4}$$

the Péclet number characterizing the strength of the flow relative to the thermal forces on the particles; and

$$\alpha = \frac{\omega b^2}{D}, \tag{5}$$

the oscillation frequency made dimensionless on the diffusive time scale. From this point forward, time and separation are made dimensionless as described.

Deviatoric stresses arise from perturbations of the pair distribution function from its equilibrium value which is unity in the semi-dilute limit. Therefore, the dimensionless Smoluchowski equation governing the microstructural response to the oscillatory flow is expressed in terms of this perturbation: $g(\mathbf{r},t) = 1 + \mathrm{Pe}\, f(\mathbf{r},t)$,

$$\dot{f} + \cos(\alpha t)\nabla \cdot [\mathbf{U}(1 + \mathrm{Pe}\, f)] = \nabla \cdot \mathbf{D} \cdot \nabla f, \tag{6}$$

with boundary conditions far from inter-particle contact ($\mathbf{r} \to \infty$), $f(\mathbf{r},t) \to 0$ and the no-flux condition at contact ($r = 2$),

$$\mathbf{r} \cdot [\cos(\alpha t)\mathbf{U}\,(1 + \mathrm{Pe}\, f) - \mathbf{D} \cdot \nabla f] = 0, \tag{7}$$

The deviatoric suspension stress will be written exclusively in terms of this deviation of the pair distribution function from equilibrium.

We expand the perturbed micro-structure, $f(\mathbf{r},t)$, as a series of harmonics of the driving frequency α such that

$$f(\mathbf{r},t) = \sum_{n=-\infty}^{\infty} e^{in\alpha t} f_n(\mathbf{r}), \tag{8}$$

and use orthogonality of the harmonics form the hierarchy of equations

$$in\alpha f_n + \frac{1}{2}\nabla \cdot \{\mathbf{U}\,[\delta_{1n} + \delta_{-1n} + \mathrm{Pe}\,\,(f_{n-1} + f_{n+1})]\} = \nabla \cdot \mathbf{D} \cdot \nabla f_n, \tag{9}$$

with

$$\hat{\mathbf{r}} \cdot \left\{ \frac{1}{2}\mathbf{U}\,[\delta_{1n} + \delta_{-1n} + \mathrm{Pe}\,\,(f_{n-1} + f_{n+1})] - \mathbf{D} \cdot \nabla f_n \right\} = 0, \tag{10}$$

at $r = 2$ and $f_n(\mathbf{r}) = 0$ as $\mathbf{r} \to \infty$. Here, δ_{1n} and δ_{-1n} are Kronecker delta functions: one if $n = 1$ or $n = -1$, respectively and zero otherwise. We previously demonstrated in the limit that $\mathrm{Pe} \to 0$,

$$f_n(\mathbf{r}) \sim O(\mathrm{Pe}^{||n|-1|}), \tag{11}$$

such that higher order structural harmonics are vanishingly small. An asymptotic expansion of the first few harmonics when $\mathrm{Pe} \ll 1$ can be written as:

$$f_0(\mathbf{r}) = \mathrm{Pe} f_0^{(1)}(\mathbf{r}) + o(\mathrm{Pe}), \tag{12a}$$

$$f_1(\mathbf{r}) = f_1^{(0)}(\mathbf{r}) + \mathrm{Pe}^2 f_1^{(2)} + o(\mathrm{Pe}^2), \tag{12b}$$

$$f_2(\mathbf{r}) = \mathrm{Pe} f_2^{(1)}(\mathbf{r}) + o(\mathrm{Pe}), \tag{12c}$$

$$f_3(\mathbf{r}) = \mathrm{Pe}^2 f_3^{(2)}(\mathbf{r}) + o(\mathrm{Pe}^2). \tag{12d}$$

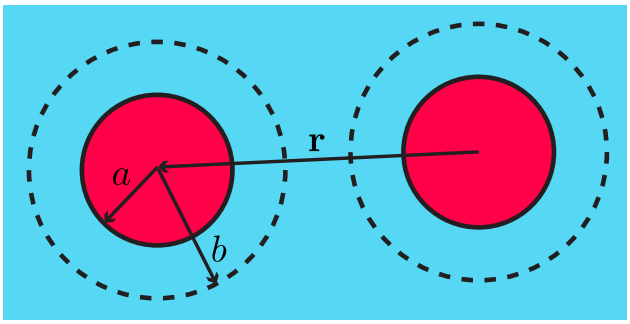

Figure 1: A pair of particles interact based on the separation between their centers $\mathbf{r}$. Each particle has a solid core of radius a at which the fluid satisfies the no-slip condition. This is the hydrodynamic radius. At separation $|\mathbf{r}| = 2b$, the particles are impenetrable to another. This is the hard-sphere interaction radius. The space between radii a and b is filled with the solvent.

In our previous paper, we solved for the linear response, $f_1^{(0)}(\mathbf{r})$, and the first departures from linearity in the microstructural perturbation, $f_0^{(1)}(\mathbf{r})$ and $f_2^{(1)}(\mathbf{r})$. Here, we will determine the leading order contribution to the third harmonic, $f_3^{(2)}(\mathbf{r})$, and the first departure from linearity in the first harmonic, $f_1^{(2)}(\mathbf{r})$. The governing equations for $f_3^{(2)}(\mathbf{r})$ and $f_1^{(2)}(\mathbf{r})$ are determined from the leading order terms with $n = 3$ and $n = 1$ in the hierarchy of microstructural equations (9 and 10):

$$3i\alpha f_3^{(2)} + \frac{1}{2}\nabla\cdot\left(\mathbf{U}f_2^{(1)}\right) = \nabla\cdot\mathbf{D}\cdot\nabla f_3^{(2)}, \tag{13}$$

$$i\alpha f_1^{(2)} + \frac{1}{2}\nabla\cdot\left[\mathbf{U}\left(f_0^{(1)} + f_2^{(1)}\right)\right] = \nabla\cdot\mathbf{D}\cdot\nabla f_1^{(2)}, \tag{14}$$

with

$$\hat{\mathbf{r}}\cdot\left[\frac{1}{2}\mathbf{U}f_2 - \mathbf{D}\cdot\nabla f_3^{(2)}\right] = 0,$$

$$\hat{\mathbf{r}}\cdot\left[\frac{1}{2}\mathbf{U}\left(f_0 + f_2\right) - \mathbf{D}\cdot\nabla f_1^{(2)}\right] = 0,$$

at $r = 2$ and $f_3^{(2)}(\mathbf{r}) \to 0$, $f_1^{(2)}(\mathbf{r}) \to 0$ as $r \to \infty$. We have already determined the quantities $f_0^{(1)}(\mathbf{r})$ and $f_2^{(1)}(\mathbf{r})$ and will not discuss their computation here. However, note that they take on the bilinear form:

$$f_{0,2}^{(1)}(\mathbf{r}) = \left(\hat{\mathbf{r}}\cdot\mathbf{E}\cdot\hat{\mathbf{r}}\right)^2\phi_{0,2}^{(1)}(r) + \left(\hat{\mathbf{r}}\cdot\mathbf{E}\cdot\mathbf{E}\cdot\hat{\mathbf{r}}\right)\chi_{0,2}^{(1)}(r) + \left(\hat{\mathbf{r}}\cdot\mathbf{\Omega}\cdot\mathbf{E}\cdot\hat{\mathbf{r}}\right)\psi_{0,2}^{(1)}(r) + \left(\mathbf{E}:\mathbf{E}\right)\xi_{0,2}^{(1)}(r). \tag{15}$$

B Inter-particle forces

In our model colloidal dispersion, the inter-particle interactions are characterized by two length scales: b, the radius at which repulsive hard sphere interaction occurs to keep the particles separated, and a, the radius at which the solvent must satisfy the no-slip condition (see figure 1). This is the excluded annulus model in which the space between the hydrodynamic radius, a, and the thermodynamic radius, b, is filled with the solvent [Morris and Brady (1996, 1997)]. The ratio $\hat{b} = b/a$ governs the strength of hydrodynamic interactions between the particles.

When $\hat{b} \to \infty$, the suspension is freely draining, so that the particles do not interact hydrodynamically. When $\hat{b} \to 1$, the hydrodynamic radii of the particles may approach asymptotically close to contact between the no-slip surfaces. Implicit in such a model is a definition for the characteristic diffusive scale D given by twice the Stokes-Einstein diffusivity, $kT/(3\pi\eta a)$ which is inversely proportional to the *hydrodynamic* radius [Einstein (1905)]. The Peclet number can be written as $\mathrm{Pe} = 3\pi\eta\dot{\Gamma}ab^2/kT$ and the dimensionless frequency as $\alpha = 3\pi\eta\omega ab^2/kT$. The

suspension stress will be calculated in the limit small particle number density, n. Thus we will account for just "pair" interactions. Results will be written in terms of the volume fraction based on the hydrodynamic radius: $\phi = 4\pi a^3 n/3$.

Hydrodynamic functions, $\mathbf{D}(\mathbf{r})$ and $\mathbf{H}(\mathbf{r})$, are written in terms of orthogonal scalar contributions:

$$\mathbf{D} = G(\hat{br})\hat{\mathbf{r}}\hat{\mathbf{r}} + H(\hat{br})\left(\mathbf{I} - \hat{\mathbf{r}}\hat{\mathbf{r}}\right) \tag{16}$$

and

$$\mathbf{H} = r\left[A(\hat{br})\hat{\mathbf{r}}\hat{\mathbf{r}} + B(\hat{br})\left(\mathbf{I} - \hat{\mathbf{r}}\hat{\mathbf{r}}\right)\right] \cdot \mathbf{E} \cdot \hat{\mathbf{r}}. \tag{17}$$

The scalar functions $G(\hat{br})$, $H(\hat{br})$, $A(\hat{br})$ and $B(\hat{br})$ are well known [Batchelor and Green (1972); Batchelor (1977)] and asymptotic expressions are given in our previous work. The advective velocity field for the particles has a finite divergence:

$$\nabla \cdot \mathbf{H} = \left[r\frac{\partial A(\hat{br})}{\partial r} + 3\left(A(\hat{br}) - B(\hat{br})\right)\right]\left(\hat{\mathbf{r}} \cdot \mathbf{E} \cdot \hat{\mathbf{r}}\right) = W(\hat{br})\left(\hat{\mathbf{r}} \cdot \mathbf{E} \cdot \hat{\mathbf{r}}\right). \tag{18}$$

A combination of analytical solutions for all of the scalar hydrodynamic functions and asymptotic expressions for nearly touching particles are used in the calculations [Jeffrey and Onishi (1984)].

C Suspension stress

The deviatoric stress in a colloidal dispersion subject to oscillatory deformation, may be written as

$$\mathbf{\Sigma}(t) = 2\eta\dot{\Gamma}\cos\alpha t\mathbf{E} + n\left(\mathbf{S}^H + \mathbf{S}^B + \mathbf{S}^P\right), \tag{19}$$

where $2\eta\dot{\Gamma}\cos(\alpha t)\mathbf{E}$ is the solvent phase stress, and the remaining three components are the deviatoric particle phase stress, called: the hydrodynamic stresslet, $\mathbf{S}^H$, the Brownian stresslet, $\mathbf{S}^B$ and the inter-particle, hard-sphere stresslet, $\mathbf{S}^P$ [Batchelor (1977)]. In the semi-dilute limit, the hydrodynamic, Brownian and hard-sphere contributions to the particle phase stress may be written in terms of $f(\mathbf{r},t)$ as [Bergenholtz, Brady and Vicic (2002)]:

$$\begin{aligned}\mathbf{S}^H = \frac{20}{3}\pi\eta a^3\dot{\Gamma}\cos(\alpha t)\Bigg\{&\left[1 + \phi\left(1 + 3\hat{b}^3\int\left(K(\hat{br}) + \frac{2}{3}L(\hat{br}) + \frac{2}{15}M(\hat{br})\right)r^2dr\right)\right]\mathbf{E} \\ &+ \frac{3\phi\hat{b}^3\mathrm{Pe}}{4\pi}\int\Bigg[K(\hat{br})\mathbf{E} + L(\hat{br})\left(\hat{\mathbf{r}}\cdot\mathbf{E}\hat{\mathbf{r}} + \hat{\mathbf{r}}\mathbf{E}\cdot\hat{\mathbf{r}} - \frac{2}{3}\left(\hat{\mathbf{r}}\cdot\mathbf{E}\cdot\hat{\mathbf{r}}\right)\mathbf{I}\right) \\ &+ M(\hat{br})\left(\hat{\mathbf{r}}\cdot\mathbf{E}\cdot\hat{\mathbf{r}}\right)\left(\hat{\mathbf{r}}\hat{\mathbf{r}} - \frac{1}{3}\mathbf{I}\right)\Bigg]f(\mathbf{r},t)d\mathbf{r}\Bigg\},\end{aligned} \tag{20a}$$

$$\mathbf{S}^B = \frac{3kT\phi\hat{b}^3\mathrm{Pe}}{8\pi}\int W(\hat{br})\left(\hat{\mathbf{r}}\hat{\mathbf{r}} - \frac{1}{3}\mathbf{I}\right)f(\mathbf{r},t)d\mathbf{r}, \tag{20b}$$

$$\mathbf{S}^P = -\frac{3kT\phi\hat{b}^3\mathrm{Pe}}{\pi}\left(1 - A(2\hat{b})\right)\int\left(\hat{\mathbf{r}}\hat{\mathbf{r}} - \frac{1}{3}\mathbf{I}\right)f(r=2,t)d\Omega, \tag{20c}$$

where $K(\hat{br}), L(\hat{br}), M(\hat{br})$ are more known hydrodynamic scalar functions for describing the hydrodynamic stresslet [Jeffrey and Onishi (1984)]. Because $f(\mathbf{r},t)$ can be written as a series of harmonics, it makes sense to expand the stresslets in the same fashion where, for $* = (H,B,P)$:

$$\mathbf{S}^* = \mathbf{S}^{*,\infty} + \sum_{n=-\infty}^{\infty} e^{in\alpha t}\mathbf{S}^*_n, \tag{21}$$

with $\mathbf{S}^{P,\infty} = \mathbf{S}^{B,\infty} = 0$ and

$$\mathbf{S}^{H,\infty} = \frac{20}{3}\pi\eta a^3\dot{\Gamma}\cos(\alpha t)\left[1 + \phi\left(1 + 3\hat{b}^3\int\left(K(\hat{br}) + \frac{2}{3}L(\hat{br}) + \frac{2}{15}M(\hat{br})\right)r^2dr\right)\right]\mathbf{E}. \tag{22}$$

In this form, the Fourier series coefficients, $\mathbf{S}_n^*$, are all linearly proportional to harmonics of the microstructural deformation. Full expressions for the $\mathbf{S}_n^*$ are given in the previous article. The leading order contributions to the third harmonic of the suspension stress are

$$\frac{\mathbf{S}_3^H}{\frac{20}{3}\pi\eta a^3\dot{\Gamma}\phi} = \frac{3\hat{b}^3\mathrm{Pe}^2}{8\pi}\int\left[K(\hat{b}r)\mathbf{E} + L(\hat{b}r)\left(\hat{\mathbf{r}}\cdot\mathbf{E}\hat{\mathbf{r}} + \hat{\mathbf{r}}\mathbf{E}\cdot\hat{\mathbf{r}} - \frac{2}{3}\left(\hat{\mathbf{r}}\cdot\mathbf{E}\cdot\hat{\mathbf{r}}\right)\mathbf{I}\right)\right. \tag{23a}$$
$$\left. + M(\hat{b}r)\left(\hat{\mathbf{r}}\cdot\mathbf{E}\cdot\hat{\mathbf{r}}\right)\left(\hat{\mathbf{r}}\hat{\mathbf{r}} - \frac{1}{3}\mathbf{I}\right)\right] f_2^{(1)}(\mathbf{r})d\mathbf{r},$$

$$\frac{\mathbf{S}_3^B}{\frac{20}{3}\pi\eta a^3\dot{\Gamma}\phi} = \frac{27\hat{b}^5\mathrm{Pe}^2}{160\pi}\int W(\hat{b}r)\left(\hat{\mathbf{r}}\hat{\mathbf{r}} - \frac{1}{3}\mathbf{I}\right) f_3^{(2)}(\mathbf{r})d\mathbf{r}, \tag{23b}$$

$$\frac{\mathbf{S}_3^P}{\frac{20}{3}\pi\eta a^3\dot{\Gamma}\phi} = -\frac{27\hat{b}^5\mathrm{Pe}^2}{20\pi}\int\left(1 - A(2\hat{b})\right)\left(\hat{\mathbf{r}}\hat{\mathbf{r}} - \frac{1}{3}\mathbf{I}\right) f_3^{(2)}(r=2)d\Omega. \tag{23c}$$

Likewise, contributions to the first departure from linearity in the first harmonic of the stress are

$$\frac{\mathbf{S}_1^H}{\frac{20}{3}\pi\eta a^3\dot{\Gamma}\phi} = \frac{3\hat{b}^3\mathrm{Pe}^2}{8\pi}\int\left[K(\hat{b}r)\mathbf{E} + L(\hat{b}r)\left(\hat{\mathbf{r}}\cdot\mathbf{E}\hat{\mathbf{r}} + \hat{\mathbf{r}}\mathbf{E}\cdot\hat{\mathbf{r}} - \frac{2}{3}\left(\hat{\mathbf{r}}\cdot\mathbf{E}\cdot\hat{\mathbf{r}}\right)\mathbf{I}\right)\right. \tag{24a}$$
$$\left. + M(\hat{b}r)\left(\hat{\mathbf{r}}\cdot\mathbf{E}\cdot\hat{\mathbf{r}}\right)\left(\hat{\mathbf{r}}\hat{\mathbf{r}} - \frac{1}{3}\mathbf{I}\right)\right]\left[f_0^{(1)}(\mathbf{r}) + f_2^{(1)}(\mathbf{r})\right]d\mathbf{r},$$

$$\frac{\mathbf{S}_1^B}{\frac{20}{3}\pi\eta a^3\dot{\Gamma}\phi} = \frac{27\hat{b}^5\mathrm{Pe}^2}{160\pi}\int W(\hat{b}r)\left(\hat{\mathbf{r}}\hat{\mathbf{r}} - \frac{1}{3}\mathbf{I}\right) f_1^{(2)}(\mathbf{r})d\mathbf{r}, \tag{24b}$$

$$\frac{\mathbf{S}_1^P}{\frac{20}{3}\pi\eta a^3\dot{\Gamma}\phi} = -\frac{27\hat{b}^5\mathrm{Pe}^2}{20\pi}\int\left(1 - A(2\hat{b})\right)\left(\hat{\mathbf{r}}\hat{\mathbf{r}} - \frac{1}{3}\mathbf{I}\right) f_1^{(2)}(r=2)d\Omega. \tag{24c}$$

Notably, higher harmonics of stresses arising from non-hydrodynamic and hydrodynamic forces have prefectures with the same scaling with respect to the Péclet number. However, these two types of stresses derive from different microstructural harmonics and thus have a different microstructural origin and character.

III Results and discussion

The results and discussion are divided into three parts: calculations of the first and third harmonics of the suspension stress as a function of α and $\hat{b}$, comparison of the theory with experimental results, and discussion of material functions capable of describing the stress state of a suspension independent of the flow geometry.

A First departures from linearity in the shear stress

We continue to consider the limit $\mathrm{Pe} \ll 1$. The $O(\mathrm{Pe}^2)$ contribution to the first and third harmonics of the suspension stress, denoted $\hat{\Delta}\boldsymbol{\Sigma}$, may be written as,

$$\hat{\Delta}\boldsymbol{\Sigma} = 10\eta\dot{\Gamma}\phi^2\left[\mathrm{Re}\,\mathbf{A}_1(\hat{b},\alpha)\cos\alpha t - \mathrm{Im}\,\mathbf{A}_1(\hat{b},\alpha)\sin\alpha t\right. \tag{25}$$
$$\left. + \mathrm{Re}\,\mathbf{A}_3(\hat{b},\alpha)\cos 3\alpha t - \mathrm{Im}\,\mathbf{A}_3(\hat{b},\alpha)\sin 3\alpha t\right],$$

where the tensors $\mathbf{A}_1(\hat{b},\alpha)$ and $\mathbf{A}_3(\hat{b},\alpha)$ are $O(\mathrm{Pe}^2)$ for all $\alpha > 0$. These tensors depend on trilinear factors of $\mathbf{E}$ or $\mathbf{\Omega}$, as

$$\begin{aligned}\mathbf{A}_{1,3} = \frac{\mathbf{S}^H_{1,3}+\mathbf{S}^B_{1,3}+\mathbf{S}^P_{1,3}}{\frac{20}{3}\pi\eta a^3\dot{\Gamma}\phi} &= I^1_{1,3}(\hat{b},\alpha)\mathbf{E}(\mathbf{E}:\mathbf{E}) + I^2_{1,3}(\hat{b},\alpha)\left(\mathbf{E}\cdot\mathbf{E}\cdot\mathbf{E} - \frac{1}{3}\mathrm{tr}(\mathbf{E}\cdot\mathbf{E}\cdot\mathbf{E})\mathbf{I}\right)\\ &+ I^3_{1,3}(\hat{b},\alpha)\left(\mathbf{\Omega}\cdot\mathbf{E}\cdot\mathbf{E} - \mathbf{E}\cdot\mathbf{E}\cdot\mathbf{\Omega}\right)\\ &+ I^4_{1,3}(\hat{b},\alpha)\left(\mathbf{\Omega}\cdot\mathbf{\Omega}\cdot\mathbf{E} + \mathbf{E}\cdot\mathbf{\Omega}\cdot\mathbf{\Omega} - \frac{2}{3}\mathrm{tr}\left(\mathbf{\Omega}\cdot\mathbf{E}\cdot\mathbf{\Omega}\right)\mathbf{I}\right)\\ &+ I^5_{1,3}(\hat{b},\alpha)\left(\mathbf{\Omega}\cdot\mathbf{E}\cdot\mathbf{\Omega} - \frac{1}{3}\mathrm{tr}\left(\mathbf{\Omega}\cdot\mathbf{E}\cdot\mathbf{\Omega}\right)\mathbf{I}\right).\end{aligned}$$

These tensors, $\mathbf{A}_1$ and $\mathbf{A}_3$ cannot be intrinsic properties of the fluid, because they depend on the flow geometry through $\mathbf{E}$ and $\mathbf{\Omega}$. Instead, the coefficients, $I^*_{1,3}(\hat{b},\alpha)$, are material functions. If the flow is simple shear, then

$$\mathbf{A}_{1,3} = \frac{1}{4}\left(2I^1_{1,3}(\hat{b},\alpha) + I^2_{1,3}(\hat{b},\alpha) - 2I^4_{1,3}(\hat{b},\alpha) + I^5_{1,3}(\hat{b},\alpha)\right)\mathbf{E}. \tag{26}$$

If it is planar extension,

$$\mathbf{A}_{1,3} = \left(2I^1_{1,3}(\hat{b},\alpha) + I^2_{1,3}(\hat{b},\alpha)\right)\mathbf{E}, \tag{27}$$

or if it is biaxial extension,

$$\mathbf{A}_{1,3} = 3\left(2I^1_{1,3}(\hat{b},\alpha) + I^2_{1,3}(\hat{b},\alpha)\right)\mathbf{E}. \tag{28}$$

Thus, knowledge of all the factors $I^*_{1,3}(\hat{b},\alpha)$ is necessary to describe the linear oscillatory flow of a non-Newtonian material in this limit. Note that in incompressible flow it can be shown that

$$\frac{1}{2}(\mathbf{E}:\mathbf{E}) = \mathbf{E}\cdot\mathbf{E}\cdot\mathbf{E} - \frac{1}{3}\mathrm{tr}(\mathbf{E}\cdot\mathbf{E}\mathbf{E})\mathbf{I}, \tag{29}$$

so that $I^1_{1,3}(\hat{b},\alpha)$ and $I^2_{1,3}(\hat{b},\alpha)$ always contribute to the stress in a proportion of 2:1. We describe these functions separately since they have distinct microstructural origins.

Figure 4 shows viscous Lissajous curves of $\hat{\mathbf{\Delta}}\mathbf{\Sigma}:\mathbf{E}$ versus the oscillatory rate of strain for oscillatory flow. These curves represent the first departure from linearity in the shear stress. Because colloidal dispersions are shear thinning in the small Pe limit at steady state, the full shear stress is expected to be smaller than the shear stress from linear response as $\alpha \to 0$. Thus, when the rate of strain is positive, the $O(\mathrm{Pe}^2)$ contribution to the shear stress is negative. The Lissajous curves have an orientation that reflects this shear thinning property.

The first and third harmonics of the $O(\mathrm{Pe}^2)$ contributions to the shear stress give rise to distinct parts of the Lissajous curves. The first harmonic can produce curves which are ellipsoidal, while the third harmonic can produce shapes having a local curvature which changes sign. Consequently, examination of both the sign of the shear stress along a Lissajous curve and the sign of the local curvature of that curve can be instructive.

As depicted in figure 3, at low frequency the sign of the Lissajous curve is predominantly opposite the sign of the rate of strain. This suggests that the real part of the first harmonic coefficient is negative. Additionally, the sign of the local curvature is opposite the sign of the rate of strain. Because the sign of the local curvature is dictated by the third harmonic, this suggests that the real part of the third harmonic coefficient is negative as well. Consequently, the first and third harmonics are shear thinning. The thinning response is characteristic of the low frequency behavior for all $\hat{b}$. However, at high frequency and for values of $\hat{b}$ near unity, the sign of the shear stress is opposite that of the rate of strain while the sign of the curvature is the same. This indicates that the first harmonic is shear thinning while the third harmonic is shear

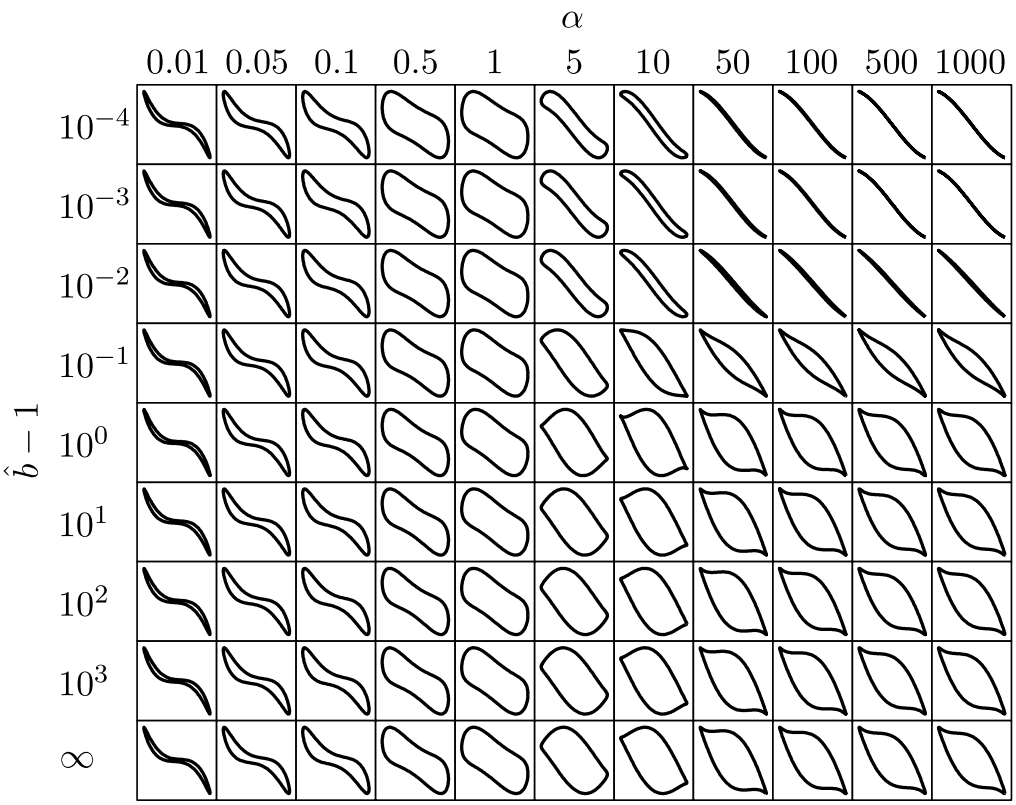

Figure 2: The $O(\mathrm{Pe}^2)$ contributions to the suspension stress in oscillatory shear flow plotted parametrically against the oscillatory rate of strain for differing values of α and $\hat{b}$. The viscous Lissajous curves are all scaled to fill each box which is centered on zero shear stress/rate of strain.

thickening. In fact the hydrodynamic forces between particles dominate the third harmonic in this limit.

The reason for this transition in behavior is the same that was discussed for linear response. The lubrication forces between particles slow their relative motion to such a degree that under high frequency oscillation, stresses in the boundary layer are suppressed. In the absence of hydrodynamic interactions, this boundary layer would lead to large stresses due to the conservative forces between particles. For particles widely separated, the microstructural perturbation vanishes. However, with strong hydrodynamic interactions the microstructural perturbation is most significant far from contact, and long-ranged hydrodynamic forces comprise the largest contribution to the suspension stress as a result.

Because hydrodynamic stresses are always at least proportional to the rate of strain in the fluid – owing to the linearity of Stokes flows – there is a fundamental difference in their scaling relative to the conservative stresses. As shown in equations 23a-23c and 24a-24c, the $O(\mathrm{Pe}^2)$ contributions to the first and third harmonics of the hydrodynamic stresslet scale with $f_2^{(1)}(\mathbf{r})$ and $f_0^{(1)}(\mathbf{r})$, which we have shown previously to possess and $O(\alpha^{-2})$ character when $\alpha \gg 1$ and $\hat{b}-1 \ll 1$. The $O(\mathrm{Pe}^2)$ contributions to the first and third harmonics of the Brownian and hard sphere stresses are proportional to $f_1^{(2)}(\mathbf{r})$ and $f_3^{(1)}(\mathbf{r})$ which can be shown to scale as α^{-3} in this same limit. Thus the hydrodynamic stresses are dominant.

In figure 4 we depict the $O(\mathrm{Pe}^2)$ contribution to Fourier coefficients of the suspension stress. These are normalized by the difference between the zero shear and high frequency viscosities of the suspension which has values: $0.913\eta\phi^2$ and $2.4\eta\hat{b}^5\phi^2$ for $\hat{b}=1$ and $\hat{b}=\infty$, respectively. At low frequency, the real parts of the first and third harmonic are negative and responsible for the

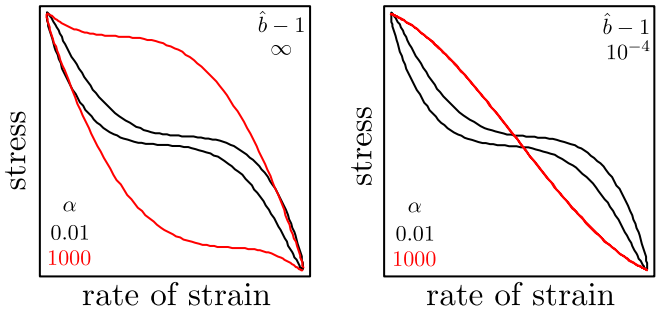

Figure 3: The $O(\mathrm{Pe}^2)$ contributions to the suspension stress in oscillatory shear flow plotted parametrically against the oscillatory rate of strain for two values of α and $\hat{b}$. The shear stress and rate of strain have been scaled by their maximum values to enable comparison of the shapes of the curves.

shear thinning response under steady shear. When $\alpha \gg 1$, however, the first and third harmonic are qualitatively dissimilar.

For the first harmonic of the shear stress, the real parts become negative at high frequency, while the imaginary parts remain positive. For $\hat{b} = \infty$, the real and imaginary parts both scale as $\alpha^{-3/2}$, while for $\hat{b}-1 = 10^{-5}$, the real part scales as α^{-2} and the imaginary part scales as α^{-3}. The consequence of this disparity is that the Lissajous curves in the absence of hydrodynamic interactions are exhibit a large hysteresis at high frequency because the real and imaginary parts of the first harmonic are the same order of magnitude. With hydrodynamic interactions, the Lissajous curves at high frequency exhibit negligible hysteresis because the real parts of the first and third harmonic are dominant. Closed Lissajous curves are indicative of a purely dissipative response which has been shown to be the only response possible for suspensions with purely hydrodynamic stresses [Swan, Zia and Brady (2014)].

For the third harmonic of the shear stress at high frequency, the real part of the Fourier coefficient is positive and scales as α^{-2} when $\hat{b} \approx 1$ while the imaginary part becomes negative and scales as α^{-3}. In the absence of hydrodynamic interactions both the real part and the imaginary part become negative and scale as $\alpha^{-3/2}$. Thus, without hydrodynamic interactions there is still a shear thinning character to the MAOS response. With hydrodynamic interactions, however, the third harmonic exhibits a shear thickening response instead. The α^{-2} scaling of this harmonic is *characteristic* of hydrodynamic stresses in the suspension. The hydrodynamic stresses driving the third harmonic is verified through comparison with measurements of the shear stress in MAOS experiments.

B Comparison with experiments

Medium amplitude oscillatory shear experiments with silica spheres (Seahoster Company, L.L.C., Japan, $a = 260$ nm at 40% particles by volume in polyethylene glycol Mw=200, $\eta = 0.049$ Pa s) were performed. Details of the sample preparation and a full rheological and microstructural characterization are published [Gurnon and Wagner (2015)]. Strain amplitude sweeps were conducted at four frequencies. The limiting behavior of the third harmonic of the shear stress at different frequencies was determined from a polynomial fit to data collected at low strain amplitude. The resulting amplitude for the third harmonic is shown in figure 5. A characteristic relaxation time of 2.8 s was measured by fitting the linear response of the dispersion to a Maxwell model. The difference between the zero shear and high frequency viscosities was found to be: $\eta_0' - \eta_\infty' = 0.73$ Pa s. The factor $|\Sigma_3^{xy}|$ represents $10\eta\dot{\Gamma}\phi^2|\mathbf{A}_3(\hat{b},\alpha) : \mathbf{E}|$ or the magnitude of the third Fourier coefficient of the shear stress The suspension exhibits a shear thickening response under steady shear, so it is assumed that $\hat{b} \approx 1$ is a suitable parameter value for comparison with the model [Bergenholtz, Brady and Vicic (2002); Maranzano and Wagner (2002)].

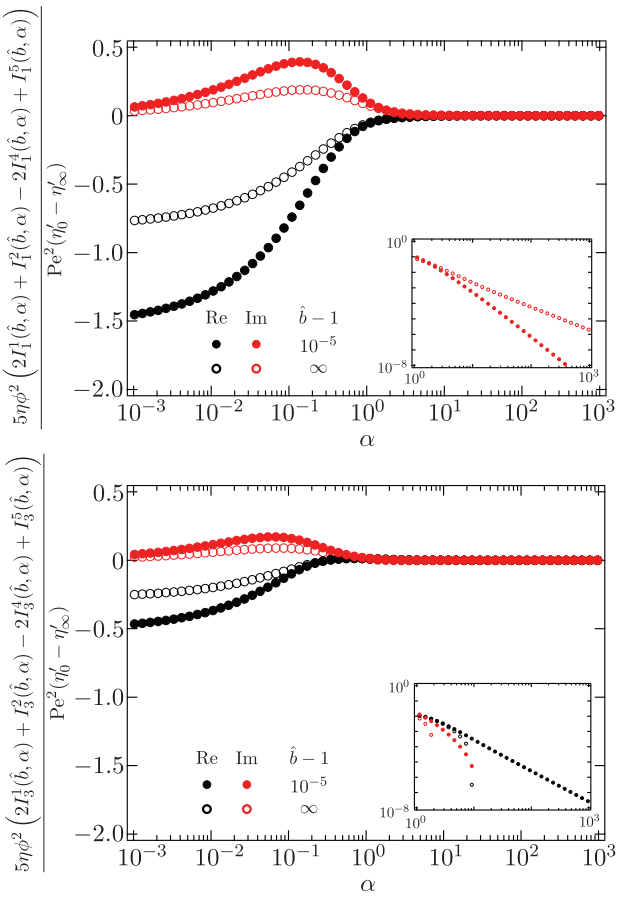

Figure 4: The $O(\mathrm{Pe}^2)$ contributions to the Fourier coefficients of the first (top) and third (bottom) harmonic of the suspension stress in oscillatory shear flow. The inset depicts the same data at high α on logarithmic scales.

In the appendix, it is shown that the microstructural harmonic $f_3^{(2)}(\mathbf{r})$ scales as α^{-3} at high frequency when $\hat{b} \approx 1$t. Additionally, prior work shows that $f_{0,2}^{(1)}(\mathbf{r})$ scales as α^{-2}. Therefore, the contributions to the third harmonic of the shear stress are predicted to scale as:

$$\frac{\mathbf{S}_3^H}{\frac{20}{3}\pi\eta a^3\dot{\Gamma}\phi} \sim \left(\frac{\mathrm{Pe}}{\alpha}\right)^2,$$

and

$$\frac{\mathbf{S}_3^B}{\frac{20}{3}\pi\eta a^3\dot{\Gamma}\phi} \sim \frac{\mathrm{Pe}^2}{\alpha^3}.$$

These divergent scaling expressions allow us to detect which of the different contributions to the suspension stress are expressed in MAOS at high frequency.

The $O(\alpha^{-2})$ scaling observed in the experiment is suggestive of hydrodynamic stresses. In studies of MAOS with other materials, a much stronger dependence on frequency has been observed Gurnon and Wagner (2012). For instance, at high frequency the third harmonic of the stress in MAOS experiments with micellar solutions and MAOS calculated from the Giesekus constitutive model both show scaling proportional to the cube of the maximum rate of strain and inversely proportional to the fourth power of frequency.

In contrast, hydrodynamically interacting suspensions produce the weaker scaling α^{-2} which results from the interaction of the microstructural deformation and the hydrodynamic stress. Because hydrodynamic stresses are always at least linear in the rate of deformation, the third

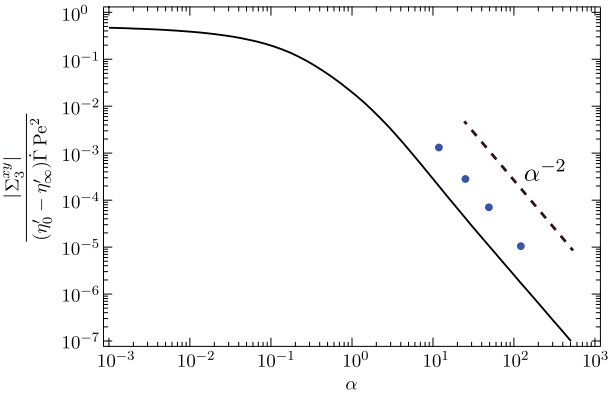

Figure 5: A comparison between experimental measurements of the third harmonic of the shear stress in a suspension of hard spheres (points) and the model calculations (solid lines).

harmonic of the hydrodynamic contribution of the stress depends on the second harmonic of the microstructural perturbation. In contrast, the conservative contributions to the third harmonic of the stress depend on the third harmonic of the microstructural perturbation.

Rescaling the frequency on the experimentally measured relaxation time and rescaling the suspension stress on $\eta_0' - \eta_\infty'$, indicates that the model has reasonable quantitative power as well. The semi-dilute model under predicts the experimental value of the third harmonic of the stress by a factor of roughly 2.5. This small difference could be attributed to the choice of relaxation time for normalization of the frequency, for instance. Alternative choices based on the short or long-time self-diffusivities of the suspended particles could be formulated. Though, we have not measured those quantities and refrain from such a comparison at present.

C Material functions for the first and third harmonic

Figures 6 and 7 present the material functions $I^*_{1,3}(\hat{b}, \alpha)$ for two limiting values of $\hat{b}$ corresponding to the limits of full and no hydrodynamic interactions. As equations 26-28 show, the stress due to uniaxial and biaxial extensional flows depends only on the material functions with $I^{1,2}_{1,3}(\hat{b}, \alpha)$. The stress in simple shear flow depends on these same functions as well as $I^{4,5}_{1,3}(\hat{b}, \alpha)$. For all values of $\hat{b}$, $I^{4,5}_{1,3}(\hat{b}, \alpha) \ll I^{1,2}_{1,3}(\hat{b}, \alpha)$ when $\alpha \gg 1$. That is, the stress response in simple shear flow approaches that of uniaxial and biaxial extension at high frequency. The rapid oscillation of the imposed flow leads to a reduced microstructural deformation related to rotational components of the simple shear flow. This same coincidence of stress responses occurs in steady shear flow at high Peclet numbers Morris and Brady (1997).

In the absence of hydrodynamic interactions, asymptotic scaling of the material functions at high frequency is directly related to which trilinear tensors they multiply. For instance, the functions: $I^{1,2}_{1,3}(\hat{b}, \alpha) \sim \alpha^{-3/2}$, and multiply trilinear terms containing three factors of $\mathbf{E}$. The function: $I^{3}_{1,3}(\hat{b}, \alpha) \sim \alpha^{-2}$, multiplies a trilinear term containing two factors of $\mathbf{E}$ and one of $\mathbf{\Omega}$. Finally, $I^{4,5}_{1,3}(\hat{b}, \alpha) \sim \alpha^{-5/2}$, multiply terms containing two factors of $\mathbf{\Omega}$ and one factor of $\mathbf{E}$. For each factor of $\mathbf{\Omega}$, the decay of the stress is stronger by $\alpha^{-1/2}$. The reason for this is that rotational flow alone cannot produce a microstructural perturbation. At high frequency, an $O(\alpha^{-1/2})$ thin boundary layer forms in the perturbed microstructure. The microstructural perturbations of lower harmonics are coupled to the higher harmonics by both straining and rotational components of the flow. However, the rotational component of the flow produces a weaker coupling and proportionally weaker stresses.

With hydrodynamic interactions, the picture at high frequency is different. $I^{1,2,3}_{1,3}(\hat{b}, \alpha)$ are all driven by hydrodynamic stresses and proportional to the second harmonic of the microstructural

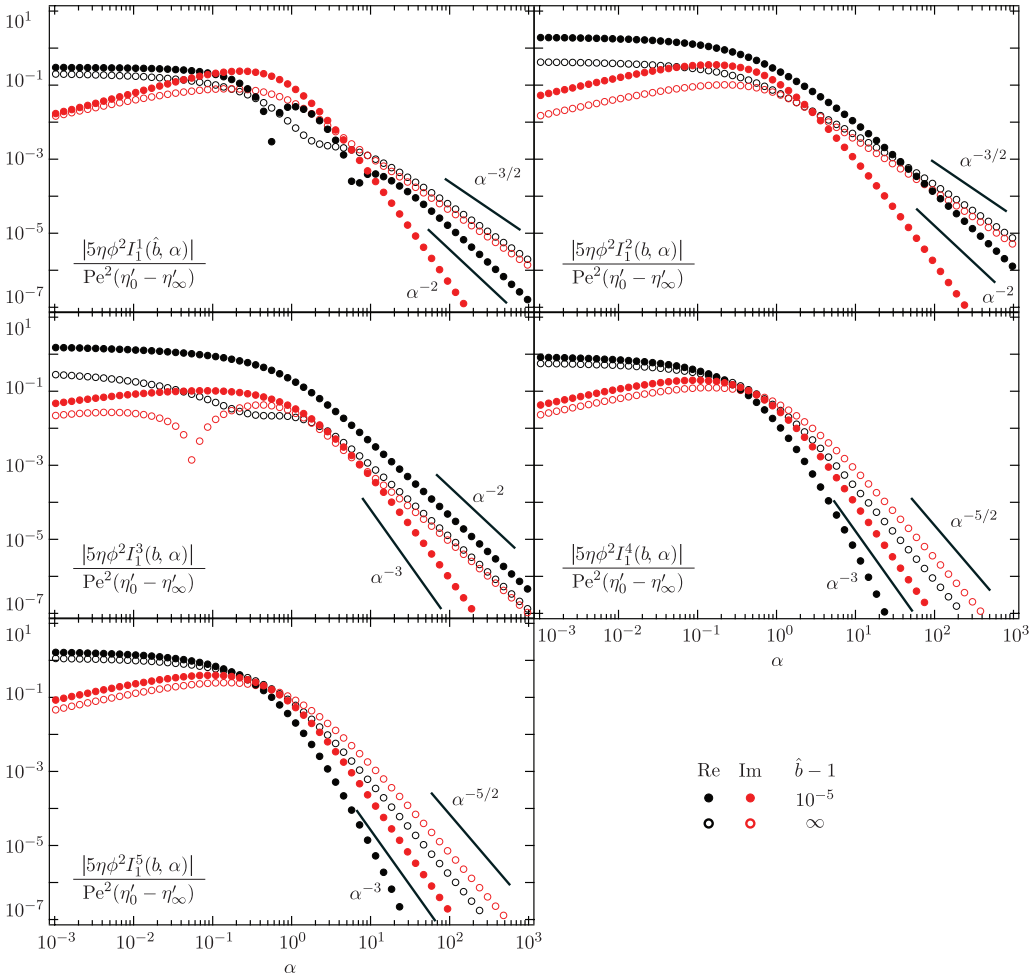

Figure 6: The material functions of the first harmonic. At small α, the real parts are all negative and the imaginary parts are all positive. With increasing α sign changes may occur which are reflected by asymptotes in a log-log plot of the absolute values of the material functions.

perturbation. We have shown that this perturbation scales as α^{-2}, and thus so do these material functions. The material functions $I_{1,3}^{4,5}(\hat{b},\alpha)$ are driven by the departures from linearity in the first and third harmonics of the microstructural perturbation instead. These material functions are entropic in origin and proportional to α^{-3} as predicted by our scaling analysis of Brownian stresses.

At low frequency with and without hydrodynamic interactions, the real parts of these material functions plateau to negative values while the imaginary parts approach zero from the positive side. The imaginary parts are proportional to $\alpha^{1/2}$ in the small α limit. This sub-linear growth rate reflects the fact that the microstructural perturbation decays to zero on a length scale proportional to $\alpha^{-1/2}$ which leads to a strong coupling of different structural harmonics in the far-field. Values for $\alpha = 0$ cannot be evaluated exactly because this coupling breaks the proposed regular perturbation scheme (eqs. 9 and 10) Brady and Vicic (1995). The limit can be extrapolated from the low frequency plateaus of the material functions instead.

For example, in steady shear flow, figure 4 suggests that the leading order contributions to the shear stress are

$$\frac{\hat{\Delta}\Sigma}{2\eta\dot{\Gamma}} \approx \frac{\eta_0'}{\eta} - \left(\frac{\eta_0'-\eta_\infty'}{\eta}\right)\mathrm{Pe}^2 \begin{cases} 1.90, & \hat{b}\to 1 \\ 1.05, & \hat{b}\to\infty \end{cases} \tag{30}$$

The extrapolated values with and without hydrodynamic interactions agree quantitatively with Bergenholtz, Brady and Vicic (2002) where this shear thinning contribution is calculated explic-

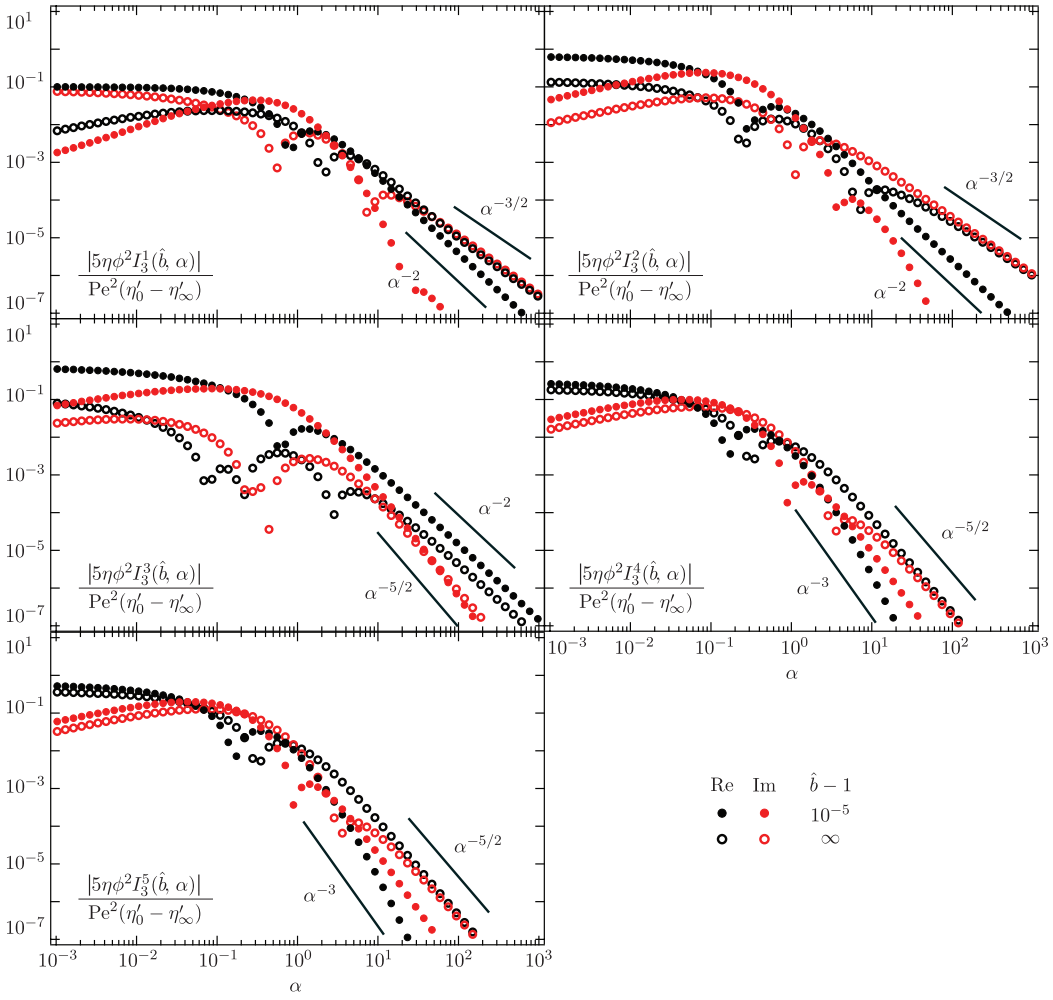

Figure 7: The material functions of the third harmonic. At small α, the real parts are all negative and the imaginary parts are all positive. With increasing α sign changes may occur which are reflected by asymptotes in a log-log plot of the absolute values of the material functions.

itly for steady shear flow. The extrapolation of $I_{1,3}^{1,2,3,4,5}(\hat{b},\alpha)$ to $\alpha = 0$ could be used to quantify the initial shear thinning of a dispersion in any flow geometry, however.

Ewoldt and Bharadwaj proposed intrinsic, nonlinear material functions that match the present MAOS description but only for shear flow [Ewoldt and Bharadwaj (2013)]. In their notation, the intrinsic functions $[e_1](\omega)$ and $[v_1](\omega)$ reflect the first elastic and viscous departures from linearity in the first harmonic, while $[e_3](\omega)$ and $[v_3](\omega)$ give the same for the third harmonic. These are related to the material functions presented here by the following relations:

$$[e_{1,3}](\omega) = -\frac{5\eta\phi^2\omega}{2\Gamma^2}\,\mathrm{Im}\left(2I_{1,3}^1(\hat{b},\alpha) + I_{1,3}^2(\hat{b},\alpha) - 2I_{1,3}^4(\hat{b},\alpha) + I_{1,3}^5(\hat{b},\alpha)\right), \tag{31}$$

$$[v_{1,3}](\omega) = \frac{5\eta\phi^2}{2\Gamma^2}\,\mathrm{Re}\left(2I_{1,3}^1(\hat{b},\alpha) + I_{1,3}^2(\hat{b},\alpha) - 2I_{1,3}^4(\hat{b},\alpha) + I_{1,3}^5(\hat{b},\alpha)\right). \tag{32}$$

Recall that the functions $I_{1,3}^*(\hat{b},\alpha)$ scale as Pe^2, so the above expressions are independent of the strain and strain-rate. They depend only on the frequency. The scaling of these functions at high frequency derived in the appendix predicts that $[e_{1,3}](\omega) \sim \omega^{-2}$, $[v_{1,3}](\omega) \sim \omega^{-2}$ when $\hat{b} \to 1$.

Finally, we note that the material function $I_{1,3}^3(\hat{b},\alpha)$ is associated with the traceless tensor: $(\mathbf{\Omega}\cdot\mathbf{E}\cdot\mathbf{E} - \mathbf{E}\cdot\mathbf{E}\cdot\mathbf{\Omega})$. This tensor is zero for all flows with a symmetric rate of strain as well as all incompressible, two dimensional flows. It is only linear flows having a three dimensional,

asymmetric rate of strain tensor that exhibit this stress response. How to measure this material function experimentally is a bit of a mystery.

D Non-linear memory functions

MAOS is important because it actively probes the nonlinear time-dependent behavior of non-Newtonian fluids. Consider just the shear stress in simple shear flow in the limit of small shear rates, which may be written as:

$$\sigma(t) = \int_{-\infty}^{\infty} A_1(t-t')\dot{\gamma}(t')dt' + \iiint_{-\infty}^{\infty} A_3(t-t',t-t'',t-t''')\dot{\gamma}(t')\dot{\gamma}(t'')\dot{\gamma}(t''')dt'dt''dt''' + \dots \tag{33}$$

By this view the shear stress is a functional of the deformation history, and this *memory kernel expansion* can be seen as a power series representation of that functional about arbitrary, but small rates of deformation. On substituting for an oscillatory shear flow, $\dot{\gamma}(t) = \dot{\gamma}_0 \cos(\omega t)$, the linear term of the memory integral expansion is proportional to:

$$\int_{-\infty}^{\infty} A_1(t-t')\dot{\gamma}(t')dt' = 2\dot{\gamma}_0 \left(\mathrm{Re}\hat{A}_1(\omega)\cos(\omega t) - \mathrm{Im}\hat{A}_1(\omega)\sin(\omega t) \right), \tag{34}$$

where $\hat{A}_1(\omega)$ is the Fourier transformation of $A_1(t)$. This is the classical linear response expression which describes how an oscillatory shear experiment can be used to extract the linear part of the memory kernel $A_1(t)$. Likewise, the cubic term becomes

$$\begin{aligned} &\iiint_{-\infty}^{\infty} A_3(t-t',t-t'',t-t''')\dot{\gamma}(t')\dot{\gamma}(t'')\dot{\gamma}(t''')dt'dt''dt''' \\ &= \frac{\dot{\gamma}_0^3}{4}\left[3\mathrm{Re}A(\omega,\omega,-\omega)\cos(\omega t) - 3\mathrm{Im}A(\omega,\omega,-\omega)\sin(\omega t)\right. \\ &\quad \left. +\mathrm{Re}A(\omega,\omega,-\omega)\cos(3\omega t) - \mathrm{Im}A(\omega,\omega,-\omega)\sin(\omega t)\sin(3\omega t)\right], \end{aligned} \tag{35}$$

where $\hat{A}_3(\omega_1,\omega_2,\omega_3)$ is the triple Fourier transformation of $A(t,t',t'')$. This shows how MAOS is capable of quantifying an additional part of the memory kernel expansion. Importantly, $\hat{A}_3(\omega,\omega,\omega)$ and $\hat{A}_3(\omega,\omega,\omega)$ are specific to the flow geometry. For simple shear deformations, these depend on a known combination of the functions $I_{1,3}^{1,2,4,5}(\hat{b},\alpha)$ that we have computed to within a constant scalar factor in figure 4.

As we have shown, the character of these material functions changes depending on the frequency from shear thinning to shear thickening. This suggests that even in the mildly nonlinear limit, the time dependent flow of hydrodynamically interacting particles can be far more complex that past retarded motion expansions would suggest Brady and Vicic (1995). Further theory and experiments exploring flows of particulate materials in complex geometries and with time varying conditions are warranted.

A modified version of MAOS can be used to access the full frequency dependence of $\hat{A}_3(\omega_1,\omega_2,\omega_3)$. If the oscillatory rate of deformation is tritone: $\dot{\gamma}(t) = \dot{\gamma}_0(\alpha_1\cos\omega_1 t + \alpha_2\cos\omega_2 t + \alpha_3\cos\omega_3 t)$, then the shear stress would feature permutations of $\hat{A}_3(\pm\omega_i,\pm\omega_j,\pm\omega_k)e^{i(\pm\omega_i\pm\omega_j\pm\omega_k)t}$. For different combinations of ω_1, ω_2 and ω_3, a complete map of $\hat{A}_3(\omega_1,\omega_2,\omega_3)$ may be constructed. Additionally, knowledge of the limiting high frequency behavior would be essential to converting this expression from the frequency domain back to the time domain. This high frequency behavior is easily assessed through analysis of microstructural relaxation much as we have demonstrated with monotone MAOS. Such an investigation is reserved for future work.

IV Conclusions

In this article, we develop a theory for predicting the first departures from linearity in the first and third harmonics of the stress from MAOS on suspensions of Brownian particles by

extending an asymptotic analysis of the suspension microstructure and stress. Varying the relative strength of the hydrodynamic interactions between suspended particles demonstrates that differing asymptotic behaviors can be expected at high frequency for freely draining and hydrodynamically interacting particles. These predictions were tested through comparison with MAOS experiments on suspensions of silica spheres which are known to shear thicken and thus interact hydrodynamically. The comparison shows the same scaling of the third harmonic of the shear stress with respect to frequency, and a scaled version of the theory predicts the magnitude of this stress signal to within a factor of 2.5. Material functions capable of describing MAOS in any flow geometry were presented as well.

We have shown that the microstructure and stress response of a non-Newtonian fluid under high frequency oscillation is highly sensitive to the physical interactions among its suspended constituents. The same must be true of all non-Newtonian fluids. The predictions made in this MAOS analysis allow for nonlinear, time-dependent rheology experiments to differentiate between stresses generated by hydrodynamic and non-hydrodynamic forces in terms of the nonlinear relaxation spectrum. A similar analysis may be paired with experiments for any microstructured material as a tool to discriminate between different physical forces driving nonlinear viscoelasticity.

Acknowledgment

NJW and AKG acknowledge support from Cooperative Agreements 70NANB10H256, and 70NANB12H239, from NIST, U.S. Department of Commerce. The statements, findings, conclusions, and recommendations are those of the author(s) and do not necessarily reflect the view of NIST or the U.S. Department of Commerce.

A Evaluation of the third harmonic of the stress

In this appendix, we extend a previous analysis of the microstructure and stress in a suspension under MAOS to the third harmonic. A slight modification of the procedure yields results for the first departures from linearity in the first harmonic as well. The appendix is organized as follows. In section 1, we describe a method for solving for the third harmonic of the suspension microstructure. In section 2 we perform an asymptotic analysis of the microstructural equations at high frequency and predict the scaling of the third harmonic of the microstructure with respect to frequency. In section 3, we provide equations for the material functions of the third harmonic of the stress in terms of harmonics of the microstructural perturbation.

1 Method of solution for the microstructural deformation

Equation 14 shows that the third harmonic of the microstructure depends linearly on the product $\mathbf{U}f_2^{(1)}(\mathbf{r})$. Because $\mathbf{U}$ is linear in the rate of strain tensor and $f_2^{(1)}(\mathbf{r})$ is bilinear in the same, the microstructural perturbation $f_3^{(2)}(\mathbf{r})$ must be trilinear in the rate of strain tensor. We write this in terms of the non-trivial trilinear products of $\mathbf{E}$ and $\mathbf{\Omega}$:

$$\begin{aligned} f_3^{(2)}(\mathbf{r}) = {} & (\hat{\mathbf{r}}\cdot\mathbf{E}\cdot\hat{\mathbf{r}})^3\,\phi_3^{(2)}(r) + (\hat{\mathbf{r}}\cdot\mathbf{E}\cdot\mathbf{E}\cdot\mathbf{r})\,(\hat{\mathbf{r}}\cdot\mathbf{E}\cdot\hat{\mathbf{r}})\,\chi_3^{(2)}(r) + (\hat{\mathbf{r}}\cdot\mathbf{\Omega}\cdot\mathbf{E}\cdot\mathbf{r})\,(\hat{\mathbf{r}}\cdot\mathbf{E}\cdot\hat{\mathbf{r}})\,\psi_3^{(2)}(r) \\ & + (\hat{\mathbf{r}}\cdot\mathbf{E}\cdot\hat{\mathbf{r}})\,(\mathbf{E}:\mathbf{E})\,\xi_3^{(2)}(r) + (\hat{\mathbf{r}}\cdot\mathbf{E}\cdot\mathbf{E}\cdot\mathbf{E}\cdot\hat{\mathbf{r}})\,\eta_3^{(2)}(r) + (\hat{\mathbf{r}}\cdot\mathbf{\Omega}\cdot\mathbf{E}\cdot\mathbf{E}\cdot\hat{\mathbf{r}})\,\theta_3^{(2)} \\ & + (\hat{\mathbf{r}}\cdot\mathbf{\Omega}\cdot\mathbf{E}\cdot\mathbf{\Omega}\cdot\hat{\mathbf{r}})\,\zeta_3^{(2)}(r) + (\hat{\mathbf{r}}\cdot\mathbf{\Omega}\cdot\mathbf{\Omega}\cdot\mathbf{E}\cdot\hat{\mathbf{r}})\,\iota_3^{(2)} + \mathrm{tr}\,(\mathbf{E}\cdot\mathbf{E}\cdot\mathbf{E})\,\mu_3^{(2)}(r) + \mathrm{tr}\,(\mathbf{\Omega}\cdot\mathbf{E}\cdot\mathbf{\Omega})\,\nu_3^{(2)}(r) \end{aligned} \tag{36}$$

The governing equations for the perturbation functions are determined by substituting the above into equation 14 and collecting like trilinear terms:

$$\frac{1}{r^2}\frac{d}{dr}\left(r^2 G(\hat{br})\frac{d}{dr}\phi_3^{(2)}\right) - \frac{42}{r^2}H(\hat{br})\phi_3^{(2)} - 3i\alpha\phi_3^{(2)} \tag{37a}$$
$$= \frac{1}{2}\left[\left(1 - A(\hat{br})\right) r\frac{d}{dr}\phi_2^{(1)} - \left(4 - 4B(\hat{br}) + W(\hat{br})\right)\phi_2^{(1)}\right]$$
$$\frac{1}{r^2}\frac{d}{dr}\left(r^2 G(\hat{br})\frac{d}{dr}\chi_3^{(2)}\right) - \frac{20}{r^2}H(\hat{br})\chi_3^{(2)} + \frac{24}{r^2}H(\hat{br})\phi_3^{(2)} - 3i\alpha\chi_3^{(2)} \tag{37b}$$
$$= \frac{1}{2}\left[\left(1 - A(\hat{br})\right) r\frac{d}{dr}\chi_2^{(1)} + 4\left(1 - B(\hat{br})\right)\phi_2^{(1)} - \left(2 - 2B(\hat{br}) + W(\hat{br})\right)\chi_2^{(1)}\right]$$
$$\frac{1}{r^2}\frac{d}{dr}\left(r^2 G(\hat{br})\frac{d}{dr}\psi_3^{(2)}\right) - \frac{20}{r^2}H(\hat{br})\psi_3^{(2)} - 3i\alpha\psi_3^{(2)} \tag{37c}$$
$$= \frac{1}{2}\left[\left(1 - A(\hat{br})\right) r\frac{d}{dr}\psi_2^{(1)} - 4\phi_2^{(1)} - \left(2 - 2B(\hat{br}) + W(\hat{br})\right)\psi_2^{(1)}\right]$$
$$\frac{1}{r^2}\frac{d}{dr}\left(r^2 G(\hat{br})\frac{d}{dr}\xi_3^{(2)}\right) - \frac{6}{r^2}H(\hat{br})\xi_3^{(2)} + \frac{2}{r^2}H(\hat{br})\chi_3^{(2)} - 3i\alpha\xi_3^{(2)} \tag{37d}$$
$$= \frac{1}{2}\left[\left(1 - A(\hat{br})\right) r\frac{d}{dr}\xi_2^{(1)} - W(\hat{br})\xi_2^{(1)}\right]$$
$$\frac{1}{r^2}\frac{d}{dr}\left(r^2 G(\hat{br})\frac{d}{dr}\eta_3^{(2)}\right) - \frac{6}{r^2}H(\hat{br})\eta_3^{(2)} + \frac{8}{r^2}H(\hat{br})\chi_3^{(2)} - 3i\alpha\eta_3^{(2)} = \left(1 - B(\hat{br})\right)\chi_2^{(1)} \tag{37e}$$
$$\frac{1}{r^2}\frac{d}{dr}\left(r^2 G(\hat{br})\frac{d}{dr}\theta_3^{(2)}\right) - \frac{6}{r^2}H(\hat{br})\theta_3^{(2)} + \frac{4}{r^2}\psi_3^{(2)} - 3i\alpha\theta_3^{(2)} = -\chi_2^{(1)} + \frac{1}{2}\left(1 - B(\hat{br})\right)\psi_2^{(1)} \tag{37f}$$
$$\frac{1}{r^2}\frac{d}{dr}\left(r^2 G(\hat{br})\frac{d}{dr}\zeta_3^{(2)}\right) - \frac{6}{r^2}H(\hat{br})\zeta_3^{(2)} - 3i\alpha\zeta_3^{(2)} = \frac{1}{2}\psi_2^{(1)} \tag{37g}$$
$$\frac{1}{r^2}\frac{d}{dr}\left(r^2 G(\hat{br})\frac{d}{dr}\iota_3^{(2)}\right) - \frac{6}{r^2}H(\hat{br})\iota_3^{(2)} - 3i\alpha\iota_3^{(2)} = -\frac{1}{2}\psi_2^{(1)} \tag{37h}$$
$$\frac{1}{r^2}\frac{d}{dr}\left(r^2 G(\hat{br})\frac{d}{dr}\mu_3^{(2)}\right) + \frac{2}{r^2}H(\hat{br})\eta_3^{(2)} - 3i\alpha\mu_3^{(2)} = 0 \tag{37i}$$
$$\frac{1}{r^2}\frac{d}{dr}\left(r^2 G(\hat{br})\frac{d}{dr}\nu_3^{(2)}\right) + \frac{2}{r^2}H(\hat{br})\left(\zeta_3^{(2)} + \iota_3^{(2)}\right) - 3i\alpha\nu_3^{(2)} = 0 \tag{37j}$$

with $\phi_3^{(2)}, \chi_3^{(2)}, \psi_3^{(2)}, \xi_3^{(2)}, \eta_3^{(2)}, \theta_3^{(2)}, \zeta_3^{(2)}, \iota_3^{(2)}, \mu_3^{(2)}, \nu_3^{(2)} \to 0$ as $r \to \infty$ and

$$G(2\hat{b})\frac{d}{dr}\phi_3^{(2)} = \left(1 - A(2\hat{b})\right)\phi_2^{(1)},\ G(2\hat{b})\frac{d}{dr}\chi_3^{(2)} = \left(1 - A(2\hat{b})\right)\chi_2^{(1)}, \tag{38}$$
$$G(2\hat{b})\frac{d}{dr}\psi_3^{(2)} = \left(1 - A(2\hat{b})\right)\psi_2^{(1)},\ G(2\hat{b})\frac{d}{dr}\xi_3^{(2)} = \left(1 - A(2\hat{b})\right)\xi_2^{(1)},\ G(2\hat{b})\frac{d}{dr}\eta_3^{(2)} = 0,$$
$$G(2\hat{b})\frac{d}{dr}\theta_3^{(2)} = 0,\ G(2\hat{b})\frac{d}{dr}\zeta_3^{(2)} = 0,\ G(2\hat{b})\frac{d}{dr}\iota_3^{(2)} = 0,\ G(2\hat{b})\frac{d}{dr}\mu_3^{(2)} = 0,\ G(2\hat{b})\frac{d}{dr}\nu_3^{(2)} = 0,$$

at $r = 2$.

It can be shown that some analytical solutions and all numerical solutions for $f_2^{(1)}$ decay exponentially fast with respect to the radial coordinate r, where the scale for the exponential decay is set by $\alpha^{-1/2}$ – that is as $\exp(-\alpha^{-1/2}r)$. The exponential decay slows as α becomes smaller so that in the limit of zero α – that is, steady flow – the exponential decay disappears and the microstructural functions decay algebraically instead.

The steady flow limit requires the use of singular perturbation techniques at this level of the approximation because the slow decay of the driving structure functions admits a convective boundary layer far from inter-particle contact Brady and Vicic (1995). However, for any finite

value of α, the exponential decay of the structure functions obviates the need for such a convective boundary layer. Because the flow oscillates, there is no time averaged advection. Therefore, $f_3^{(2)}$ may be determined through numerical solution of the preceding equations on a radial domain which is large relative to the $\alpha^{-1/2}$ length scale for the exponential decay. We utilize the boundary collocation method *bvp4c* in MATLAB to solve this system of boundary value problems.

2 High frequency asymptotic analysis of the microstructure

In the limit of high frequency, diffusion may be considered irrelevant to leading order. Time variation of the microstructural perturbation balances the oscillatory advection over most of the domain. Therefore, eliminating diffusive terms from equations 37a-37j

$$\phi_3^{(2)}(r) = \frac{i}{6\alpha}\left[\left(1 - A(\hat{br})\right) r\frac{d}{dr}\phi_2^{(1)}(r) - \left(4 - 4B(\hat{br}) + W(\hat{br})\right)\phi_2^{(1)}(r)\right] \tag{39a}$$

$$\chi_3^{(2)}(r) = \frac{i}{6\alpha}\left[\left(1 - A(\hat{br})\right) r\frac{d}{dr}\chi_2^{(1)}(r) + 4\left(1 - B(\hat{br})\right)\phi_2^{(1)}(r) - \left(2 - 2B(\hat{br}) + W(\hat{br})\right)\chi_2^{(1)}(r)\right] \tag{39b}$$

$$\psi_3^{(2)}(r) = \frac{i}{6\alpha}\left[\left(1 - A(\hat{br})\right) r\frac{d}{dr}\psi_2^{(1)}(r) - 4\phi_2^{(1)}(r) - \left(2 - 2B(\hat{br}) + W(\hat{br})\right)\psi_2^{(1)}(r)\right] \tag{39c}$$

$$\xi_3^{(2)}(r) = \frac{i}{6\alpha}\left[\left(1 - A(\hat{br})\right) r\frac{d}{dr}\xi_2^{(1)}(r) - W(\hat{br})\xi_2^{(1)}(r)\right] \tag{39d}$$

$$\eta_3^{(2)}(r) = \frac{i}{3\alpha}\left(1 - B(\hat{br})\right)\chi_2^{(1)}(r) \tag{39e}$$

$$\theta_3^{(2)}(r) = \frac{i}{3\alpha}\left[-\chi_2^{(1)}(r) + \frac{1}{2}\left(1 - B(\hat{br})\right)\psi_2^{(1)}(r)\right] \tag{39f}$$

$$\zeta_3^{(2)}(r) = \frac{i}{6\alpha}\psi_2^{(1)}(r) \tag{39g}$$

$$\iota_3^{(2)}(r) = -\frac{i}{6\alpha}\psi_2^{(1)}(r) \tag{39h}$$

$$\mu_3^{(2)}(r) = 0 \tag{39i}$$

$$\nu_3^{(2)}(r) = 0 \tag{39j}$$

These equations fail to satisfy the no flux boundary condition at contact, however. Near contact, there is a boundary layer where diffusion balances the time variation of the structure. The character of the boundary layer depends on the strength of the hydrodynamic interactions.

In our previous article we showed that $\phi_2^{(1)}(r)$, $\chi_2^{(1)}(r)$, $\psi_2^{(1)}(r)$ and $\xi_2^{(1)}(r)$ are all real and proportional to α^{-2} outside the boundary layer. Therefore, the functions making up the third harmonic contribution to the microstructural perturbation are to leading order imaginary and at most $O(\alpha^{-3})$ in this same outer region. Note, in the absence of hydrodynamic interactions, these functions are identically zero in the outer region since the strictly affine motion of particles far from contact will produce no microstructural perturbation at all.

In the absence of hydrodynamic interactions, the width of the boundary layer is proportional to $\alpha^{-1/2}$. Defining a new boundary layer coordinate $y = \alpha^{-1/2}(r-2)$ allows us to focus on the small region in which the oscillating flow is balanced by diffusive fluxes. Recalling that $\phi_2^{(1)} \sim \alpha^{-1}$, $\xi_2^{(1)}, \psi_2^{(1)} \sim \alpha^{-3/2}$, and $\xi_2^{(1)} \sim \alpha^{-5/2}$ in the boundary layer, and by retaining only

the leading order terms, the microstructural perturbation equations become:

$$\frac{d^2}{dy^2}\phi_3^{(2)} - 3i\phi_3^{(2)} = \alpha^{-1/2}\frac{d}{dy}\phi_2^{(1)} \tag{40a}$$

$$\frac{d^2}{dy^2}\chi_3^{(2)} - 3i\chi_3^{(2)} = \alpha^{-1/2}\frac{d}{dy}\chi_2^{(1)} \tag{40b}$$

$$\frac{d^2}{dy^2}\psi_3^{(2)} - 3i\psi_3^{(2)} = \alpha^{-1/2}\frac{d}{dy}\psi_2^{(1)} \tag{40c}$$

$$\frac{d^2}{dy^2}\xi_3^{(2)} - 3i\xi_3^{(2)} = \alpha^{-1/2}\frac{d}{dy}\xi_2^{(1)} \tag{40d}$$

$$\frac{d^2}{dy^2}\eta_3^{(2)} - 3i\eta_3^{(2)} = \alpha^{-1}\chi_2^{(1)} \tag{40e}$$

$$\frac{d^2}{dy^2}\theta_3^{(2)} - 3i\theta_3^{(2)} = -\alpha^{-1}\chi_2^{(1)} + \frac{1}{2}\alpha^{-1}\psi_2^{(1)} \tag{40f}$$

$$\frac{d^2}{dy^2}\zeta_3^{(2)} - 3i\zeta_3^{(2)} = \frac{1}{2}\alpha^{-1}\psi_2^{(1)} \tag{40g}$$

$$\frac{d^2}{dy^2}\iota_3^{(2)} - 3i\iota_3^{(2)} = -\frac{1}{2}\alpha^{-1}\psi_2^{(1)} \tag{40h}$$

$$\frac{d^2}{dy^2}\mu_3^{(2)} + \frac{1}{2}\alpha^{-1}\eta_3^{(2)} - 3i\mu_3^{(2)} = 0 \tag{40i}$$

$$\frac{d^2}{dy^2}\nu_3^{(2)} + \frac{1}{2}\alpha^{-1}\left(\zeta_3^{(2)} + \iota_3^{(2)}\right) - 3i\nu_3^{(2)} = 0. \tag{40j}$$

These boundary layer equations are sufficient to show that $\phi_3^{(2)} \sim \alpha^{-3/2}$, $\xi_3^{(2)}, \psi_3^{(2)} \sim \alpha^{-2}$, $\zeta_3^{(2)} \sim \alpha^{-3}$, $\eta_3^{(2)}, \theta_3^{(2)}, \iota_3^{(2)} \sim \alpha^{-5/2}$, and $\mu_3^{(2)}, \nu_3^{(2)} \sim \alpha^{-7/2}$. Substituting these scalings into the integrals for the material functions (41-45) validates the scaling observed in figure 7 at high frequency.

When $\hat{b} \approx 1$, the boundary layer thickness scales at α^{-1} instead. The thinner boundary layer arises because relative motion between nearly touching particles is suppressed by lubrication interactions. Consequently, within the $O(\alpha^{-1})$ boundary layer, $f_1^{(0)} \sim \alpha^{-1}$, $f_{0,2}^{(1)} \sim \alpha^{-2}$ and $f_{1,3}^{(2)} \sim \alpha^{-3}$. The stresses arising from the microstructural perturbations in the boundary layer are smaller than those arising from the outer, slow diffusion region. Thus boundary layer stresses are negligible when hydrodynamic interactions are strong.

3 Calculation of the material functions for the third harmonic of the stress

The material functions for the third harmonic of the stress (25) can be written in terms of the bilinear and trilinear microstructural perturbations as:

$$I_3^1(\hat{b},\alpha) = \mathrm{Pe}^2\left\{\frac{1}{210}\hat{b}^3\int_2^\infty \Big[3K(\hat{b}r)\left(14\phi_2^{(1)}(r)+35\chi_2^{(1)}(r)+105\xi_2^{(1)}(r)\right) \right. \tag{41}$$
$$+6L(\hat{b}r)\left(2\phi_2^{(1)}(r)+7\chi_2^{(1)}(r)+35\xi_2^{(1)}(r)\right)+2M(\hat{b}r)\left(2\phi_2^{(1)}(r)+3\chi_2^{(1)}(r)+21\xi_2^{(1)}(r)\right)\Big]r^2dr$$
$$+\frac{3}{700}\hat{b}^5\int_2^\infty W(\hat{b}r)\left[2\phi_3^{(2)}(r)+3\chi_3^{(2)}(r)+21\xi_3^{(2)}(r)\right]r^2dr$$
$$\left.-\frac{6}{175}\hat{b}^5(1-A(2\hat{b}))\left[2\phi_3^{(2)}(2)+3\chi_3^{(2)}(2)+21\xi_3^{(2)}(2)\right]\right\},$$
$$I_3^2(\hat{b},\alpha) = \mathrm{Pe}^2\left\{\frac{1}{105}\hat{b}^3\int_2^\infty \left[6L(\hat{b}r)\left(4\phi_2^{(1)}(r)+7\chi_2^{(1)}(r)\right)+M(\hat{b}r)\left(8\phi_2^{(1)}(r)+12\chi_2^{(1)}(r)\right)\right]r^2dr\right.$$
$$+\frac{3}{700}\hat{b}^5\int_2^\infty W(\hat{b}r)\left[8\phi_3^{(2)}(r)+12\chi_3^{(2)}(r)+21\eta_3^{(2)}(r)\right]r^2dr$$
$$\left.-\frac{6}{175}\hat{b}^5(1-A(2\hat{b}))\left[8\phi_3^{(2)}(2)+12\chi_3^{(2)}(2)+21\eta_3^{(2)}(2)\right]\right\}, \tag{42}$$
$$I_3^3(\hat{b},\alpha) = \mathrm{Pe}^2\left\{\frac{1}{70}\hat{b}^3\int_2^\infty \left[7L(\hat{b}r)+2M(\hat{b}r)\right]\psi_2^{(1)}(\hat{b}r)r^2dr \right. \tag{43}$$
$$\left.+\frac{9}{1400}\hat{b}^5\int_2^\infty W(\hat{b}r)\left[2\psi_3^{(2)}(r)+7\theta_3^{(2)}(r)\right]r^2dr-\frac{9}{175}\hat{b}^5(1-A(2\hat{b}))\left[2\psi_3^{(2)}(2)+7\theta_3^{(2)}(2)\right]\right\},$$
$$I_3^4(\hat{b},\alpha) = \mathrm{Pe}^2\left\{\frac{9}{200}\hat{b}^5\int_2^\infty W(\hat{b}r)\iota_3^{(2)}(r)r^2dr-\frac{9}{25}\hat{b}^5(1-A(2\hat{b}))\iota_3^{(2)}(2)\right\}, \tag{44}$$
$$I_3^5(\hat{b},\alpha) = \mathrm{Pe}^2\left\{\frac{9}{100}\hat{b}^5\int_2^\infty W(\hat{b}r)\zeta_3^{(2)}(r)r^2dr-\frac{18}{25}\hat{b}^5(1-A(2\hat{b}))\zeta_3^{(2)}(2)\right\}. \tag{45}$$

These terms are evaluated numerically with a trapezoidal method applied to the integrals.

The leading departure from linearity of the first harmonic exhibits identical scaling to the third harmonic and may be determined through a similar analysis of the microstructural equations. For brevity, we describe a simple reconstruction procedure. First, substitute $\phi_0^{(1)}+\phi_2^{(1)}$ for $\phi_2^{(1)}$ and $\phi_1^{(2)}$ for $\phi_3^{(2)}$ in equations 37a-37j for the microstructural perturbation. Do the same for all the other structural modes ($\chi,\psi,\xi,$, *etc.*). Then, replace all occurrences of 3α by α to build the equations for the first departures from linearity of the perturbed microstructure. The same series of substitutions can be applied to equations 41-45 along with replacing I_3^* with I_1^* to produce equations for the first harmonic material functions of the stress.

References

Atalik K. and R. Keunings. On the occurrence of even harmonics in the shear stress response of viscoelastic fluids in large amplitude oscillatory shear. *J. Non-Newtonian Fluid Mech.* **122**, 107–116 (2004).

Batchelor G.K. and J.T. Green. The hydrodynamic interaction of two small freely-moving spheres in a linear flow field. *J. Fluid Mech.* **56**(2), 375–400 (1972).

Batchelor G.K. The effect of Brownian motion on the bulk stress in a suspension of spherical particles. *J. Fluid Mech.* **83**, 97–117 (1977).

Bender J. and N.J. Wagner. Reversible shear thickening in monodisperse and bidisperse colloidal dispersions. *J. Rheol.* **40**, 899–916 (1996).

Bergenholtz J., J.F. Brady and M. Vicic. The non-Newtonian rheology of dilute colloidal suspensions. *J. Fluid Mech.* **456**, 239–275 (2002).

Bird R., R. Armstrong, and O. Hassager. *Dynamics of Polymeric Liquids: Volume 1 Fluid Mechanics*. Wiley, New York (1987).

Bird, R. B., A.J. Giacomin, A.M. Schmalzer, and C. Aumnate. Dilute rigid dumbbell suspensions in large-amplitude oscillatory shear flow: Shear stress response. J. of Chem. Phys., **140**(7), 074904 (2014).

Brady J.F. and G. Bossis. Stokesian Dynamics. *Ann. Rev. of Fluid Mech.*, **20**, 111–157 (1988).

Brady J.F. The rheological behavior of concentrated colloidal dispersions. *J. Chem. Phys.* **99**(1), 567–581 (1993).

Brady J.F. and M. Vicic. Normal stresses in colloidal dispersions. *J. Rheol.* **39**(3), 545–566 (1995).

Brady J.F. and N.J. Wagner. Shear thickening in colloidal dispersions. *Phys. Today* **62**(10), 27–32 (2009).

Cho K.S., K.H. Ahn, and S.J. Lee. A geometrical interpretation of large amplitude oscillatory shear response. *J. Rheol* **49**, 747–758 (2005).

Cox W.P. and E.H. Merz. Correlation of dynamic and steady flow viscosities. *J. Poly. Sci.* **28**(118), 619–622 (1958).

Dealy, J.M., and K.F. Wissbrun. *Melt Rheology and Its Role in Plastics Processing: Theory and Applications* Van Nostrand Reinhold, New York (1990).

Doraiswamy D., A.N. Mujumdar, I. Tsao, A.N. Beris, S.C. Danforth and A.B. Metzner. The CoxÐMerz rule extended: A rheological model for concentrated suspensions and other materials with a yield stress. *J. Rheol.* **35**(4) (1991).

Einstein A.E. Über die von der molekularkinetischen theorie der tärme geforderte bewegung von in ruhenden flüssigkeiten suspendierten teilchen. *Annalen der Physik* 322, 549–560 (1905).

Ewoldt R.H, A.E. Hosoi and G.H. McKinley. New measures for characterizing nonlinear viscoelasticity in large amplitude oscillatory shear. *J. Rheol.* **52** 1427–1458 (2008).

Ewoldt, R. H., and N.A. Bharadwaj. Low-dimensional intrinsic material functions for nonlinear viscoelasticity. *Rheo. Acta*, **52**(3), 201–219 (2013).

Giacomin, A.J., and J.M. Dealy. Large-amplitude oscillatory shear, chap. 4 in *Techniques in Rheological Measurement* edited by A. A. Collyer. Elsevier Applied Science, London (1993).

Giacomin, A. J., and R.B. Bird. Normal stress differences in large-amplitude oscillatory shear flow for the corotational ÒANSRÓ model. *Rheo. Acta*, **50**(9-10), 741–752 (2011).

Gurnon A.K. and N.J. Wagner. Large amplitude oscillatory shear (LAOS) measurements to obtain constitutive equation model parameters: Giesekus model of banding and nonbanding wormlike micelles. *J. Rheol.* **56**(2), 333–351 (2012).

Gurnon, A. K., C.R. Lopez-Barron, A.P. Eberle, L. Porcar, and N.J. Wagner. Spatiotemporal stress and structure evolution in dynamically sheared polymer-like micellar solutions. *Soft Matter*, **10**(16), 2889–2898 (2014).

Gurnon, A.K. Nonlinear oscillatory rheology and structure of wormlike micellar solutions and colloidal suspensions. University of Delaware, Ph.D. thesis (2014).

Gurnon, A.K. and N.J. Wagner Microstructure and rheology relationships for shear thickening colloidal dispersions. *J. Fluid Mech.*, **769**, 242–276 (2015).

Hyun K., S.H. Kim, K.H. Ahn and S.J. Lee. Large amplitude oscillatory shear as a way to classify the complex fluids. *J. Non-Newtonian Fluid Mech.* **107** 51–65 (2002).

Hyun, K., M. Wilhelm, C.O. Klein, K.S. Cho, J.G. Nam, K.H. Ahn, and G.H. McKinley. A review of nonlinear oscillatory shear tests: Analysis and application of large amplitude oscillatory shear (LAOS). *Prog. in Polymer Sci.*, **36**(12), 1697–1753 (2011).

Jeffrey D.J. and Y. Onishi. Calculation of the resistance and mobility functions for two unequal rigid spheres in low-Reynolds-number flow. *J. Fluid Mech.* **139**, 261–290 (1984).

Jeffrey D.J. The calculation of the low Reynolds number resistance functions for two unequal spheres. *Phys. Fluids A* **4**, 16–29 (1992).

Kim S. and S.J. Karrila. *Microhydrodynamics: Principles and Selected Applications.* Dover, Mineola (2005).

Kim, J. M., A.P. Eberle, A.K. Gurnon, L. Porcar, and N.J. Wagner. The microstructure and rheology of a model, thixotropic nanoparticle gel under steady shear and large amplitude oscillatory shear (LAOS). *J. Rheology*, **58**(5), 1301–1328 (2014).

Larson R.G. *The Structure and Rheology of Complex Fluids.* Oxford University Press, New York (1999).

Lee Y.S., E.D. Wetzel and N.J. Wagner. The ballistic impact characteristics of Kevlar woven fabrics impregnated with a colloidal shear thickening fluid. *J. Mat. Sci.* **38**, 2935–2833 (2003).

Lionberger, R. A. and W. B. Russel. High frequency modulus of hard spheres. *J. Rheol.* **38**, 1885–1908 (1994).

López-Barrón C.R., L. Porcar, A.P.R. Eberle and N.J. Wagner. Dynamics of melting and recrystallization in a polymeric micellar crystal subjected to large amplitude oscillatory shear flow. *Phys. Rev. Lett.* **108**(25), 258301 (2012).

Maranzano B.J. and N.J. Wagner. Flow-small angle neutron scattering measurements of colloidal dispersion microstructure evolution through the shear thickening transition. *J. Chem. Phys.* **117**, 10291–10302 (2002).

Mewis J. and N.J. Wagner. *Colloidal Suspension Rheology.* Cambridge University Press, Cambridge (2012).

Morris J.F. and J.F. Brady. Self diffusion in sheared suspensions. *J. Fluid Mech.*, **312**, 223–252, (1996).

Morris J.F. and J.F. Brady. Microstructure of strongly sheared suspensions and its impact on rheology and diffusion. *J. Fluid Mech.*, **348**, 103–139 (1997).

Phung T.N., J.F. Brady and G. Bossis. Stokesian Dynamics simulation of Brownian suspensions. *J. Fluid Mech.* **313**, 181–207 (1996).

Pipkin A.C. *Lectures on Viscoelasticity Theory.* Springer-Verlag, New York (1986).

Rogers S.A. and M.P. Lettinga. A sequence of physical processes determined and quantified in large-amplitude oscillatory shear (LAOS): Application to theoretical nonlinear models. *J. Rheol.* **56**, 1–25 (2012).

Rogers S.A., J. Kohlbrecher and M.P. Lettinga. The molecular origin of stress generation in worm-like micelles, using a rheo-SANS LAOS approach. *Soft Matter* **8**, 7831–7839 (2012).

W. B. Russel, D. A. Saville, and W. R. Schowalter. *Colloidal Dispersions*. Cambridge University Press, 1989.

Shikata T. and D.S. Pearson. Viscoelastic behavior of concentrated spherical suspensions. *J. Rheol.* **38**, 601–616 (1994).

Swan J.W., E.M. Furst and N.J. Wagner. A physical model for fitting the linear viscoelastic spectrum of colloidal dispersions. *Rheoacta* in submission (2013).

Swan J.W., E.M. Furst and N.J. Wagner. The medium amplitude oscillatory shear (MAOS) of semi-dilute colloidal dispersions, part 1: linear response and normal stress differences. *J. Rheology* **58**, 307–338 (2014).

Swan J.W., R.N. Zia and J.F. Brady. Large amplitude oscillatory micorheology. *J. Rheology* **58**, 1–41 (2014).

van der Werff, J.C., C.G. de Kruif, C. Blom and J. Mellema. Linear viscoelastic behavior of dense hard-sphere dispersions. *Phys. Rev. A* **39**, 418– (1989).

Wagner N.J. and A.T.J. Woutersen. The viscosity of bimodal and polydisperse suspensions of hard spheres in the dilute limit. *J. Fluid Mech.* **278** 267–287 (1994).

Wilhelm W. Fourier-transform rheology. *Macromol. Mater. Eng.* **287** 83–105 (2002).